Available online at www.sciencedirect.com

ScienceDirect

Surface & Coatings Technology 202 (2008) 3017 – 3022

SURFACE & COATINGS TECHNOLOGY

www.elsevier.com/locate/surfcoat

Corrosion behavior and surface characterization of tantalum implanted TiNi alloy

Yan Li [a,*], Songbo Wei [a], Xiangqian Cheng [b,c], Tao Zhang [b,c], Guoan Cheng [b,c]

[a] *School of Material Science and Engineering, Beijing University of Aeronautics and Astronautics, Beijing 100083, China*
[b] *Key Lab of Radiation Beam Technology and Material Modification, National Ministry of Education of China, Beijing Normal University, Beijing 100875, China*
[c] *Institute of Low Energy Nuclear Physics, Beijing Normal University, Beijing 100875, China*

Received 3 July 2007; accepted in revised form 3 November 2007
Available online 12 November 2007

Abstract

TiNi shape memory alloy has been modified by Ta plasma immersion ion implantation technology to improve corrosion resistance. The results of the polarization tests show that the corrosion resistance of TiNi alloy in Ringer's solution at 310 K has been improved by the Ta ion implantation and the Ta/TiNi sample with a moderate incident dose of 1.5×10^{17} ions/cm^2 exhibits the best corrosion resistance ability. The surface characterization and chemical composition of the Ta/TiNi samples were determined by Auger electron spectroscopy (AES), Atomic force microscopy (AFM) and X-ray photoelectron spectroscopy (XPS) methods. AFM images reveal that compact aggregates of nano-grains uniformly disperse on the surface of the Ta/TiNi samples. AES and XPS analyses on the Ta/TiNi sample show that the component of the surface layer is mainly composed of TiO_2 and Ta_2O_5, which is benefit to the corrosion resistance ability and biocompatibility.
© 2007 Elsevier B.V. All rights reserved.

Keywords: PIII; TiNi; Tantalum; Corrosion

1. Introduction

TiNi shape memory alloys (SMA) are well-known smart materials with excellent shape memory effect and pseudoelasticity [1,2]. Moreover, they have been successfully applied in many medical aspects due to good corrosion resistance ability and biocompatibility [3]. It is known that the release of toxic Ni ion from TiNi alloy may cause allergic reactions and promote carcinogenesis [4]. Therefore, many methods of surface modification including magnetron sputtering [5], thermally oxidizing [6], hydrothermal synthesis [7] and ion implantation [8], have been performed on TiNi alloy to improve its surface passivation. By ion implantation technology, e.g. plasma based ion implantation (PBII) and plasma immersion ion implantation (PIII), some nonmetallic elements, boron [9], phosphorus[10], carbon [11,12], nitrogen [9,12] and oxygen [8,13] have been implanted into TiNi alloys and thus remarkably improved the anti-corrosion ability as well as surface mechanical properties.

Tantalum (Ta) is one of the most important metallic biomaterials and is often used as film material to improve the performance of substrate because of its excellent biocompatibility and high corrosion resistance [14,15]. Recently, the improvement of corrosion resistance ability of TiNi in 0.9% NaCl solution modified by Ta PIII has been reported [15]. In the present work, the TiNi alloy was modified by Ta PIII at different incident doses. The relationship between the incident dose and the corrosion resistance ability of the TiNi and Ta implanted TiNi samples in Ringer's solution has been investigated by potentiodynamic anodic polarization tests associated with the analyses of the surface morphologies and chemical states.

2. Experimental methods

2.1. Sample preparation

The nominal composition of the alloy is Ti-50.6 at.% Ni. The phase transformation behavior of the alloy was determined by a

* Corresponding author. Tel.: +86 10 82315989; fax:+86 10 82338200.
E-mail address: liyan@buaa.edu.cn (Y. Li).

0257-8972/$ - see front matter © 2007 Elsevier B.V. All rights reserved.
doi:10.1016/j.surfcoat.2007.11.003

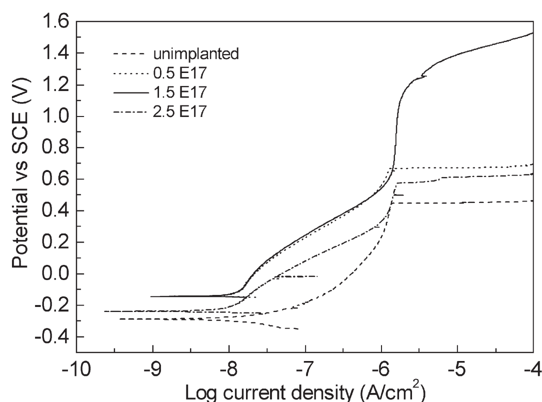

Fig. 1. Potentiodynamic anodic polarization curves of the TiNi and the Ta implanted samples with different incident doses in Ringer's solution.

Perkin-Elmer DSC-7 with a cooling/heating rate 10 K/min, the martensitic transformation start temperature (M_s) and the reverse martensitic transformation finish temperature (A_f) of the TiNi alloy are measured as 240 K and 257 K, respectively. All samples were cut from the TiNi alloy plate to a size of 10 mm × 10 mm × 1 mm and polished progressively with 340–2000 grits SiC emery papers and then mirror polished with diamond paste.

2.2. Ta implantation

Prior to implantation, samples were ultrasonically cleaned in acetone and anhydrous ethanol for 10 min respectively, and then were put into PIII chamber. The vacuum chamber was evaluated to a base pressure of 5×10^{-4} Pa and then samples were sputtered with energetic argon ions at −5 kV to remove residual surface contaminants. The implanted target material was pure Ta (99.99%). The surface modification process employing Ta MEVVA plasma source was carried out at −45 kV bias voltage with ion current of 2 mA. In order to reveal the effects of incident dose on the electrochemical behavior and evaluate the best corrosion resistance, three values for incident ion dose, i.e. 0.5×10^{17}, $1.5\times10^{17}$and 2.5×10^{17} ions/cm^2 were chosen in this work.

2.3. Electrochemical tests

Electrochemical experiments were performed on 10 mm× 10 mm square TiNi specimens in Ringer's solution (pH = 7.4) [16]: 9.00 g/l NaCl, 0.20 g/l $NaHCO_3$, 0.25 g/l $CaCl_2{\cdot}6H_2O$, 0.4 g/l KCl. Potentiodynamic polarization tests were carried out using a computer-controlled electrochemical analytic equipment (Shanghai Chenhua equipment company, model CHI 604A) with a standard three-electrode system. A saturated calomel electrode (SCE) was used as the reference electrode and a platinum electrode acted as counter electrode. Polarization measurements started after the samples immersed in the Ringer's solution for 20 min under open-circuit conditions. The potential scan started at 100 mV more cathodic than open-circuit potential (OCP), increasing towards the anodic values at a constant rate of 1 mV/s, and stopped until the breakdown potential (E_{br}) was achieved. All electrochemical tests were performed at 310 K.

2.4. Surface characterization

A multimode Atomic Force Microscopy (AFM) from Veeco Metrology was employed for surface observations. Elemental depth profiling analysis was performed with a PHI 700 (ULVAC-PHI, Japan) Auger electron spectroscopy (AES). The pressure of the analysis chamber was lower than 1.9×10^{-9} Torr. All AES measurements were carried out with a 5 keV primary electron beam with an analytical spot diameter of 50 μm. Surface chemical composition and states were determined by X-ray photoelectron spectroscopy (XPS, PHI Quantera SXM, ULVAC-PHI). A monochromatic Al Kα (1486.6 eV) X-ray source at 25 W was used with an analytical spot diameter of 100 μm and a 45° takeoff angle, with pass energy of 55 eV. An argon ion gun was employed to sputter the surface of sample. The binding energy scale was calibrated to the C1 s peak at 284.8 eV.

3. Results and discussion

3.1. Corrosion analyses of the Ta implanted TiNi alloys

The polarization curves of TiNi and Ta implanted TiNi samples in Ringer's solution at 310 K (pH = 7.4) are shown in Fig. 1. It is clearly seen that the corrosion behavior of TiNi was affected by Ta ion implantation. The corrosion potential (E_{corr}), the breakdown potential (E_{br}) and the corrosion current density (i_{corr}) are listed in Table 1 to evaluate the corrosion resistance of the samples, where i_{corr} is calculated by the Stern-Geary equation as described in [17]. The E_{br} corresponding to the onset of pitting corrosion is usually at potential marked by a rapid increase of the passive current density, and the higher the E_{br} is, the less susceptible the alloy is to initiate pitting corrosion. Both of E_{corr} and E_{br} increase for the three Ta implanted samples and the maximum of them are displayed in the 1.5×10^{17} ions/cm^2 dose sample. The maximum of E_{br} of the Ta implanted TiNi sample is about 600 mv higher than that of TiNi alloy with TiN coating made by powder immersion reaction assisted coating annealed at 1173 K [16]. Moreover, even with a higher Cl^- concentration in our Ringer's solution, the maximum of E_{br} is about 400 mv higher than that of Ta implanted TiNi in 0.9% NaCl solution as reported by Cheng et al. [15]. i_{corr} of the samples remarkably decreases after Ta implantation and the values are very close to each other for the Ta implanted samples. The minimum of i_{corr} is 9.7×10^{-9} A/cm^2 in our Ta implanted

Table 1
Results from electrochemical tests for the TiNi sample and the Ta implanted samples

Sample	E_{corr} (mV)	E_{br} (mV)	i_{corr}(A/cm^2)
Unimplanted	−288	450	8.7×10^{-8}
0.5E17	−145	671	1.04×10^{-8}
1.5E17	−141	1299	1.01×10^{-8}
2.5E17	−239	581	9.7×10^{-9}

sample, which is superior to those of DLC (Diamond-like carbon) film coated TiNi [18]. The lower i_{corr} means that the Ta implanted samples would be eroded more slowly than the unimplanted sample. Based on the above analysis, it can be concluded that the Ta implanted sample with a moderate incident ion dose of the 1.5×10^{17} ions/cm^2 exhibits the best corrosion resistance.

3.2. Surface morphologies of the Ta implanted TiNi alloys

Fig. 2 shows the AFM images for the surface of the TiNi and the Ta implanted samples. There are many grooves on the surface of the TiNi sample, which were fabricated by polishing process, as shown in Fig. 2a. For each Ta implanted sample, the surface layer is composed of compact aggregates of grains with a mean size of about 10 nm. Similar to the results of the oxygen ion implanted TiNi alloy [8], grooves on the TiNi sample were removed by Ta implantation, indicating the inhibition the beginning of pitting corrosion for TiNi. The mean surface roughness R_a of the 1.5×10^{17} ions/cm^2 Ta implanted sample is about 8.45 nm, which is very close to that reported in Ref. [15]. The other two Ta implanted samples appear more acute surfaces, suggesting the easiness to suffering pitting corrosion. This is consistent with the results of polarization tests.

3.3. Chemical and structure analyses of the Ta ion implanted TiNi alloys

The Auger depth profiles of the TiNi and Ta/TiNi (specializes to the 1.5×10^{17} ions/cm^2 Ta ion implanted TiNi) samples are shown in Fig. 3. The element distribution on depth scale was calculated according to the sputtering rates from a SiO_2 reference under similar condition. It is known that the sputtering rate of TiNi is different from that of SiO_2 and thus the depth profiles in Fig. 3 are approximate, but comparison among different samples is more valid [7,12]. The high concentration of carbon at the surface for both TiNi and Ta/TiNi samples are due to environmental contamination as commonly reported. It is seen from Fig. 3a that a high concentration of oxygen is present on the surface of TiNi and diminishes rapidly with depth, because Ti has a high affinity for oxygen and can form oxide films spontaneously in an oxygenated environment. However, the concentrations vs. depth of nickel and titanium show inverse variation feature of oxygen and reach an approximate 50:50 Ni: Ti ratio at 130 nm. This result is similar to that in ref. [7].

It is known that the amount of Ni in the surface and the atomic ratio Ni/Ti at the surface are important quantities reflecting the toxicity of the surface [7]. For Ta implanted the TiNi sample, it is reasonable to evaluate toxicity of the surface with atomic ratio Ni/(Ti+Ta). The surface elemental

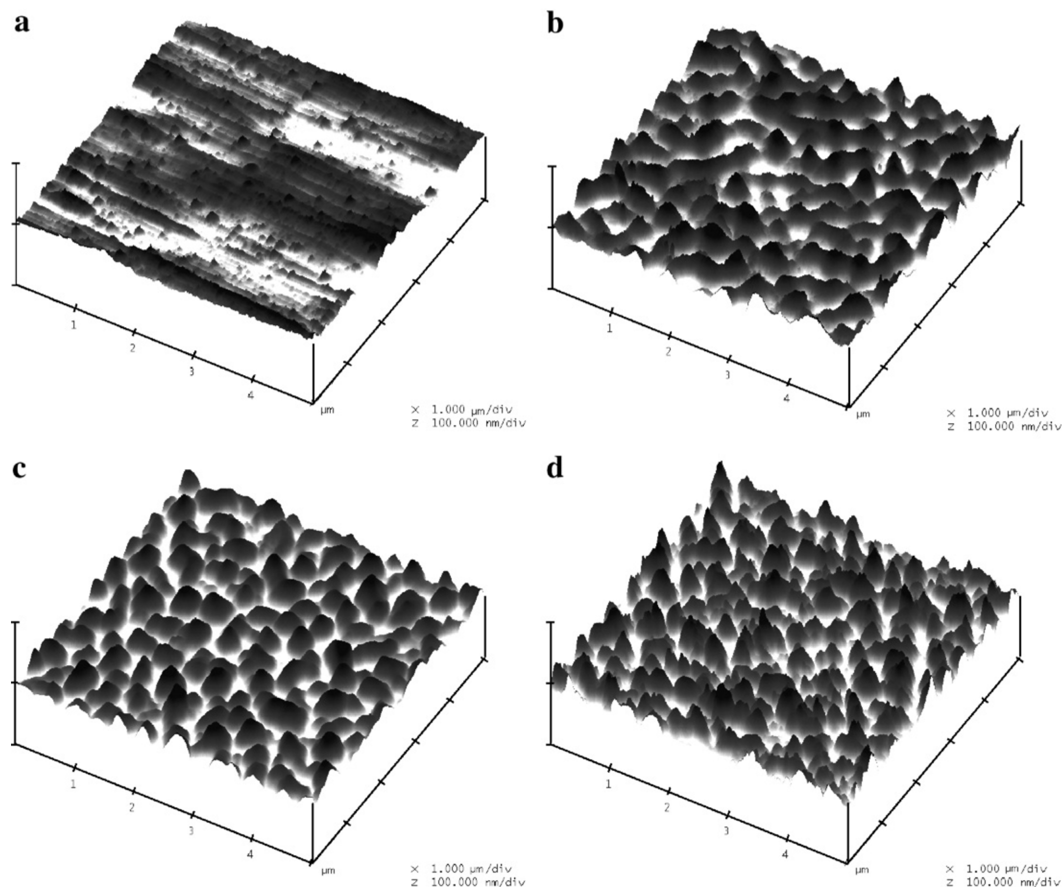

Fig. 2. Atomic force images for the surface of (a) the TiNi sample and the Ta implanted TiNi samples with incident dose of (b) 0.5×10^{17}, (c) 1.5×10^{17} and (d) 2.5×10^{17} ions/cm^2.

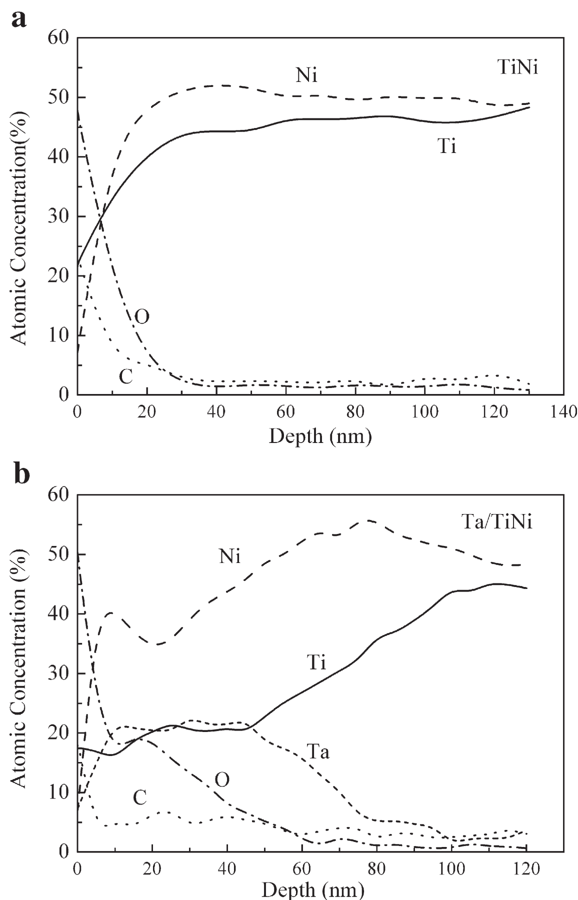

Fig. 3. Auger peak-to-peak depth profiles of (a) the TiNi sample and (b) the Ta/TiNi sample.

compositions of the TiNi and the Ta/TiNi samples calculated from AES spectra are listed in Table 2. It is believed that the Ta/TiNi sample should exhibit better biocompatibility than the TiNi sample with relatively lower Ni surface composition and Ni/(Ti+Ta) of 6.78 and 0.27, respectively. Furthermore, it is noted that Ni concentration of the Ta/TiNi sample is reduced from 54% to 40% in subsurface, meaning a potentially reduction of the risk of nickel liquefying from bulk TiNi.

The Auger depth profiles of the Ta/TiNi sample are more complex as shown in Fig. 3b. Ta concentration has an approximate Gaussian distribution with a peak concentration at 21%, which is much higher than the maximum of Ta concentration (12%) in Ta implanted TiNi reported in ref [15], and thus the Ta contained layer can be divided into three parts due to different atomic concentrations, i.e. the surface (0–10 nm), the subsurface (10–50 nm) and the inner (50–100 nm). It should be pointed out that oxygen was inevitably implanted to the subsurface, because the PIII process was conducted in the non-UHV (ultra high vacuum) conditions [19]. The atomic concentration of oxygen falls rapidly from 47% to 20% in the surface, and then falls slowly in the subsurface till to approximate zero in the inner. Comparing with the TiNi sample, the Ta/TiNi exhibits significant differences on the Ti and Ni atomic concentration distribution. Ti concentration almost keeps the same level around 20% in the surface and subsurface, and then slowly rises to 40% in the inner. Ni concentration rises to 40% more rapidly than that of TiNi sample in the surface, falls to 35% in the subsurface, and reaches the maximum of 55% in the inner. Similar depth profiles of Ti and Ni can be found in the carbon ion implanted TiNi (40 kV C_2H_2 implantation without annealing) in ref [12]. This is due to the sputtering effect of Ta PIII. When Ta ions were implanted to the TiNi surface, Ti and Ni ions were sputtered and most of the incident Ta ions remained in the subsurface (10–50 nm). Therefore, parts of Ni atoms were moved from the subsurface layer to the surface layer leading to a more rapid increase in the depth profile of Ta/TiNi sample and, simultaneously, a part of Ti atoms were drove out from the subsurface into the surface layer leading to the similar concentration level in them.

In order to determine the chemical states of O, Ni, Ta and Ta elements in depth of Ta/TiNi sample, the high-resolution XPS spectra of O1 s, Ni2p, Ti 2p and Ta 4f are measured at a series of sputtering time as shown in Fig. 4. It is seen from Fig. 4a that two primary peaks of O1 s at 530.5 and 532.0 eV remain on the surface without sputtering, indicating metal oxide bonds and absorbent oxygen bonds, respectively [20]. After Ar^+ sputtering for 3 min (about 2 nm depth in the surface, calculated by the Ar^+ sputtering rate as shown in the caption of Fig. 4.), only metal oxide bonds remain, and O1 s peaks become weak with the increasing of the sputtering time indicating the reduction of oxygen quantity in depth. There is no evident $Ni2p_{3/2}$ peak on the surface as shown in Fig. 4b, but small amount of Ni should exist here as indicated by AES result in Fig. 3b. The chemical states of Ti 2p on the surface without sputtering are doublet consisting of 2p1/2 at 464.4 eV and 2p3/2 at 458.7 eV, respectively, as shown in Fig. 4c. This result indicates that TiO_2 is a main component in the surface layer of Ta/TiNi samples. In the Ar^+ sputtering period from 3 min (2 nm depth in the surface) to 6 min (39 nm depth in the subsurface), the Ti2p peaks become complex, which is attributed to the coexistence of variable of Ti bonds such as Ti^{2+} (TiO) and $Ti3^+$ (Ti_2O_3) [7], while only the metallic Ti^0 peaks ($Ti^0 2p_{3/2}$ at 454.1 eV and $Ti^0 2p_{1/2}$ at 460.3 eV) are detected after Ar^+ sputtering for 9 min (76 nm depth in the inner). It is seen from Fig. 4d that on the surface the doublet peaks at low bonding energy side (very weak) and the doublet peaks at high bonding energy side correspond to Ta^0 (metallic Ta) and Ta^{5+} (Ta_2O_5), respectively [21], and the former are enhanced at the expanse of the latter after Ar^+ sputtering for 3 min (2 nm depth in the surface). After Ar^+ sputtering for 4 min (14.4 nm depth in the subsurface), only metallic Ta can be seen in the XPS spectra. Therefore, the surface of the Ta/TiNi sample is predominantly covered by a

Table 2
Surface composition (at.%) of the TiNi sample and the Ta/TiNi sample

	C	O	Ni	Ti	Ta	Ni/(Ti+Ta)
TiNi	22.98	47.13	7.63	21.55	0	0.35
Ta/TiNi	18.66	49.84	6.78	17.57	7.24	0.27

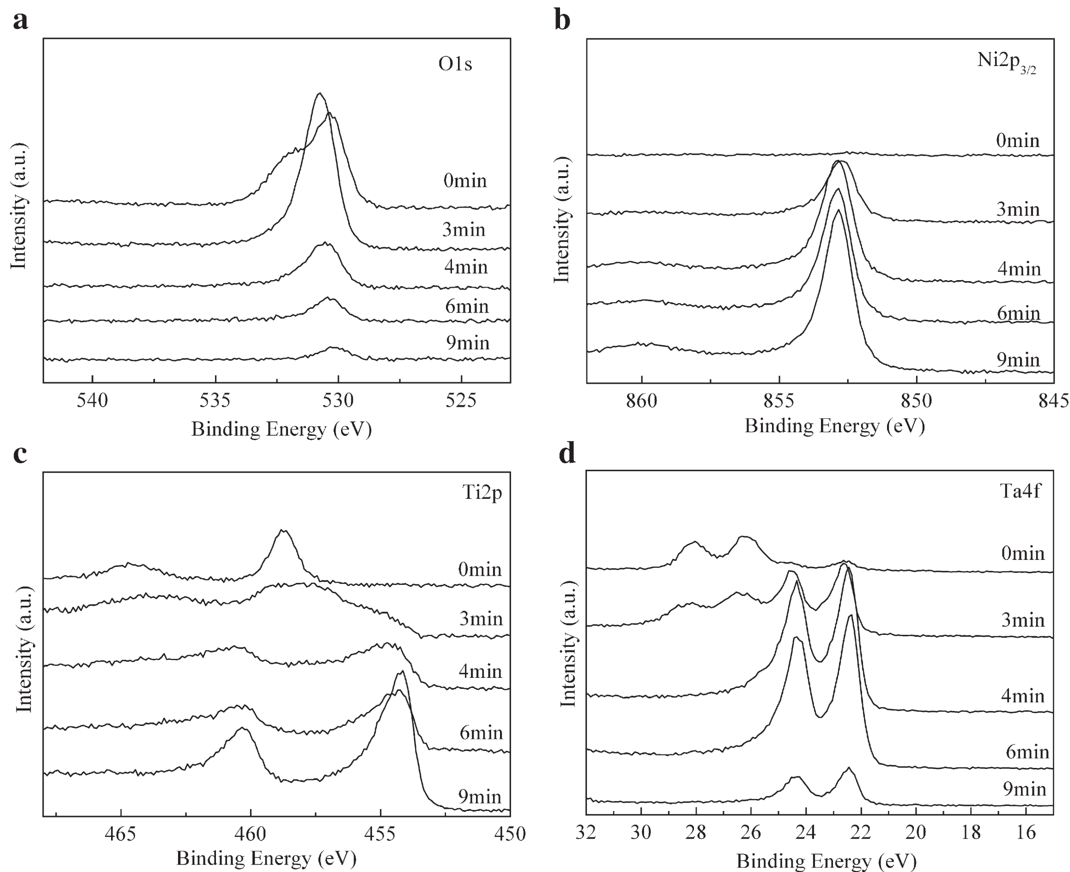

Fig. 4. High-resolution XPS spectra of (a) O1 s, (b) $Ni2p_{3/2}$, (c) Ti2p and (d) Ta4f of the Ta/TiNi sample, Ar^+ sputtering Rate = 0.67 nm/min (0–3 min), 12.4 nm/min (>3 min) for SiO_2.

composite layer composed of TiO_2 and Ta_2O_5 with small amounts of Ta and Ni, while in the subsurface of 10–50 nm depth, the metallic Ti, Ni and Ta coexist with TiO_2. According to above analyses, it can be concluded that the primary reason for the improvement of corrosion resistance of Ta ion implanted TiNi alloy is the formation of a composite surface layer composed of TiO_2 and Ta_2O_5.

4. Conclusions

In summarization, TiNi alloy has been modified by Ta implantation and corrosion resistance behaviors in Ringer's solution are investigated. The results show that a composite TiO_2/Ta_2O_5 surface layer forms in the state of compact aggregates of nano-grains on Ta implanted TiNi alloy, which is more stable than a pure TiO_2 passive layer in corrosive medium. The corrosion resistance of TiNi alloy in Ringer's solution has been improved by Ta implantation. Ta implanted sample with a moderate incident ion dose of 1.5×10^{17} ions/cm^2 exhibits the best corrosion resistance due to its relatively slippery surface morphology.

Acknowledgement

This work is supported by the Science Foundation of Key Lab of Radiation Beam Technology and Material Modification, National Ministry of Education of China. Yan Li acknowledges funding by Beijing Nova Program (BNP) and by Program for Changjiang Scholars and Innovative Research Team in University (PCSIRT) (IRT0512).

References

[1] K. Otsuka, C.M. Wayman editor, Shape Memory Materials, Cambridge University Press, Cambridge, 1998.
[2] K. Otsuka, X. Ren, Prog. Mater. Sci. 50 (2005) 511.
[3] T. Duerig, A. Pelton, D. Stockel, Mater. Sci. Eng., A Struct. Mater.: Prop. Microstruct. Process. 273–275 (1999) 149.
[4] M. Uo, F. Watari, A. Yokoyama, H. Matsuno, T. Kawasaki, Biomaterials 20 (1999) 747.
[5] L.F. Senna, C.A. Achete, T. Hirsch, F.L. Freire Jr, Surf. Coat. Technol. 94–95 (1997) 390.
[6] Y.W. Gu, B.Y. Tay, C.S. Lim, M.S. Yong, Appl. Surf. Sci. 252 (2005) 2038.
[7] M.H. Wong, F.T. Cheng, H.C. Man, Scr. Mater. 56 (2007) 205.
[8] L. Tan, R.A. Dodd, W.C. Crone, Biomaterials 24 (2003) 3931.
[9] H. Pelletier, D. Muller, P. Mille, J.J. Grob, Surf. Coat. Technol. 158-159 (2002) 309.
[10] X.K. Zhao, W. Cai, L.C. Zhao, Surf. Coat. Technol. 155 (2002) 236.
[11] Y. Cheng, Y.F. Zheng, Surf. Coat. Technol. 201 (2007) 4909.
[12] R.W.Y. Poon, K.W.K. Yeung, X.Y. Liu, P.K. Chu, C.Y. Chung, W.W. Lu, K.M.C. Cheung, D. Chan, Biomaterials 26 (2005) 2265.
[13] L. Tan, W.C. Crone, K. Sridharan, J. Mater. Sci., Mater. Med. 13 (2002) 501.
[14] J.Y. Chen, Y.X. Leng, X.B. Tian, L.P. Wang, N. Huang, P.K. Chu, P. Yang, Biomaterials 23 (2002) 2545.

[15] Y. Cheng, C. Wei, K.Y. Gan, L.C. Zhao, Surf. Coat. Technol. 176 (2004) 261.
[16] D. Starosvetsky, I. Gotman, Biomaterials 22 (2001) 1853.
[17] M. Koike, Z. Cai, H. Fujii, M. Brezner, T. Okabe, Biomaterials 24 (2003) 4541.
[18] Y. Cheng, Y.F. Zheng, Surf. Coat. Technol. 200 (2006) 4543.
[19] Ray W.Y. Poon, Joan P.Y. Ho, X.Y. Liu, C.Y. Chung, Paul K. Chu, Kelvin W.K. Yeung, William W. Lu, Kenneth M.C. Cheung, Mater. Sci. Eng., A Struct. Mater.: Prop. Microstruct. 390 (2005) 444.
[20] L. Tan, W.C. Crone, Acta Mater. 50 (2002) 4449.
[21] G.H. Yu, C.L. Chai, H.C. Zhao, F.W. Zhu, J.M. Xiao, J. Magn. Magn. Mater. 224 (2001) 61.